Catalysis Today 155 (2010) 27–34

Contents lists available at ScienceDirect

Catalysis Today

journal homepage: www.elsevier.com/locate/cattod

Fuel-rich methane combustion over Rh-$LaMnO_3$ honeycomb catalysts

G. Landi [a], P.S. Barbato [b], S. Cimino [a,*], L. Lisi [a], G. Russo [b]

[a] Istituto Ricerche sulla Combustione – CNR – P.le V. Tecchio 80, 80125, Napoli, Italy
[b] Dipartimento Ingegneria Chimica – Università degli Studi di Napoli Federico II, Italy

ARTICLE INFO

Article history:
Available online 14 February 2009

Keywords:
Catalytic combustion
Partial oxidation
Rh
Perovskite
Honeycomb morphology
Methane

ABSTRACT

Structured catalysts with mixed Rh-$LaMnO_3$ formulation were developed for the partial oxidation of methane to syngas intended as a preliminary conversion step in advanced combustion systems such as power turbines and utility burners employing a catalytic fuel-rich approach to reduce thermal NO_x formation. Honeycomb catalysts were fully characterized by ICP-MS, BET, DRIFT, H_2-TPR and their performances were tested under self-sustained, high temperature catalytic partial oxidation reaction to assess the impact of noble metal loading. Moreover, at fixed catalyst formulation, the impact of substrate morphology and thermal conductivity was addressed by direct comparison of honeycombs with several cell densities (cordierite 200–1200 cpsi) and two solid materials (cordierite vs. SiC).

1. Introduction

Catalytic combustion is perceived as a viable technology to carry out stable and efficient fuel oxidation at lower temperatures, compared to a conventional flame, thus preventing pollutants formation [1]. The most active catalysts for lean methane combustion are based on noble metals, in particular palladium, although they suffer from deactivation phenomena at moderate-high temperatures related to sintering and/or decomposition and show unstable, oscillating behaviours. The inability of the catalytic system to fulfil all process requirements has led to complex process designs including additional homogeneous or catalytic stages and, in turn, has limited a wide diffusion of catalytic combustion in power and heat production [2].

Fuel-rich catalytic combustion has been recently proposed as a preliminary conversion stage for gas turbine burners. In this process, a fuel-rich/air mixture is catalytically converted to both partial and total oxidation products that are subsequently mixed with excess air to complete the combustion in an ultra-lean homogeneous flame [3]. The presence of syngas in the hot product stream from the catalytic zone can help in stabilizing lower temperature flames in the burnout zone, thus reducing NO_x emissions [3]. Further advantages are related to an intrinsically safer operation of the fuel-rich catalytic stage which is not prone to flashback issues, and to the non-sooting characteristic of the diluted syngas secondary flame, regardless of the specific fuel fed to the first catalytic stage. From the point of view of the catalytic system, the moderate extent of the catalytic reaction, due to the limited oxygen availability, prevents the catalyst from reaching very high temperatures even in the presence of a not perfectly mixed feed, thus preventing deactivation and significantly improving its durability [3]. Moreover, the absence of adsorbed surface oxygen minimizes catalyst volatilization as noble metal oxide [3].

Several studies have reported that catalytic partial oxidation of methane and higher hydrocarbons can yield near complete conversion to mostly H_2 and CO in short contact time structured catalytic reactors running autothermally [4–9]. Catalysts with high Rh loadings onto ceramic foams honeycombs or spheres provided the best performances compared to Pd, Pt or Ni based systems in terms of light-off temperature, H_2 yields, stability against volatilization, resistance to carbon deposition [10]. The addition of Rh to a perovskite phase has been recently proposed in order to better disperse the noble metal, thus reducing its required amount (i.e. the cost), and to stabilize it in a wider range of temperatures [11]. Moreover, the synergy due to the simultaneous presence of total oxidation and reforming active sites in the same catalytic system has been shown to reduce light-off temperature, enhance methane conversion and inhibit coke formation [11].

The prolonged high rhodium prices (3–5 times that of Pt) due to steadily increasing demand for use in gasoline catalytic converters [12] has encouraged to extend research into the impact of reduction in noble metal loading for Rh-$LaMnO_3$ catalysts supported over La-stabilized alumina [11]. Structured honeycomb catalysts were fully characterized by ICP-MS, BET, DRIFT, H_2-TPR and their performance in the partial oxidation of methane/air mixtures was tested under self-sustained, high temperature operating conditions. Moreover, at fixed catalyst formulation,

* Corresponding author. Tel.: +39 081 7682233; fax: +39 081 5936936.
E-mail address: stefano.cimino@cnr.it (S. Cimino).

0920-5861/$ – see front matter © 2009 Elsevier B.V. All rights reserved.
doi:10.1016/j.cattod.2009.01.020

the impact of substrate morphology and thermal conductivity was addressed by direct comparison of honeycombs with several cell densities (cordierite 200–1200 cpsi) and two solid materials (cordierite vs. SiC).

2. Experimental

$LaMnO_3$ perovskite and Rh precursor salts were deposited by incipient wetness impregnation [11] onto an intermediate La_2O_3-stabilized γ-Al_2O_3 washcoat layer of constant nominal average thickness (20 μm), which was anchored on monolith substrates. Commercial honeycombs with straight, parallel channels of roughly square cross-section, made by extruded cordierite ($2MgO{\cdot}2Al_2O_3{\cdot}5SiO_2$), were provided by Saint-Gobain Ceramics (200 cpsi), Corning (400 cpsi), and NGK (600, 900, 1200 cpsi); honeycombs made of oxide bonded SiC-91% were obtained from CTI (190, 290 cpsi).

The target loading of active phase in the washcoat layer (monolithic substrate excluded) was ~30% (w/w) perovskite and 0.1%, 0.5% or 1% (w/w) Rh. Reference powder catalysts with same composition were prepared by incipient wetness impregnations of the La-γ-Al_2O_3 powder used as washcoat for the monoliths. All the catalysts were calcined in air at 800 °C for 3 h.

In the following Rh-$LaMnO_3$ catalysts are labelled as LMR-*x*-*y*, where *x* is the nominal Rh content and *y* represents the cell density of the honeycomb substrate in the case of structured samples.

2.1. Catalyst characterization

Actual metal content was quantitatively determined on selected fresh and used catalysts by inductively coupled plasma spectrometry (ICP) on an Agilent 7500 ICP-MS instrument, after microwave-assisted digestion of samples in nitric/hydrochloric acid solution.

XRD analysis was performed using a PW 1100 Philips XRD diffractometer with CuKα radiation.

BET specific surface area of monolith samples, evaluated by N_2 adsorption at 77 K using a Quantachromm Autosorb 1-C after degassing under vacuum at 150 °C, was assigned only to the active washcoat layer (SSA of honeycomb substrate $\leq$1 m^2/g).

H_2-TPR experiments were carried out on powder catalysts and selected monoliths (crushed) with Micrometrics TPD/TPR 2900 apparatus equipped with a TCD. Samples were pre-treated at 800 °C under air flow for 1 h before the experiment, and then reduced with a 2% H_2/Ar mixture (25 cm^3 min^{-1}), heating at 10 °C min^{-1} from room temperature up to 800 °C.

DRIFT experiments were performed on a PerkinElmer Spectrum GX spectrometer with a spectral resolution of 4 cm^{-1}. LMR-1 and LMR-0.1 powder samples were placed in a high temperature Pike DRIFT cell equipped with a ZnSe window and connected to mass flow controlled gas lines. Spectra of the samples, pre-oxidized *in-situ* at 800 °C, were recorded under reaction conditions (100 cm^3 min^{-1} of a CH_4/O_2/Ar mixture (26/15/59)) from 300 to 800 °C. After cooling down to room temperature CO was adsorbed (2% CO/N_2) for 30 min and spectra were taken after Ar purging. Spectra of adsorbed CO at room temperature were also recorded after reducing *in-situ* the samples with a 2% H_2/N_2 mixture for 30 min at 450 °C (roughly corresponding to the end of the main TPR signal) or 800 °C. Spectra of the corresponding oxidized samples taken at same temperature under Ar flow were used as background in any case.

2.2. Catalyst testing

The catalytic monoliths, in the shape of disks of 17 mm diameter and 10 mm long, were stacked between two inert mullite foams (45 ppi, l = 12 mm) which served as radiation shields and were placed in a quartz tube inserted in an electric furnace that was used for pre-heating the reacting mixture. Reactor temperatures were measured by means of sheathed K-type thermocouples in the centre of each monolith and in the exit gas after the last radiation shield, at the beginning of the reactor cooling zone, which prolongs outside of the external furnace [11,13]. The thermocouple in the catalytic honeycomb had its tip (0.5–1 mm) placed in close contact with the solid wall and the gas flow in the measuring channel was strongly reduced due to the presence of the thermocouple itself: therefore the temperature reading in the honeycomb catalyst (T_{cat}) is believed to be more indicative of the surface temperature, although, in general, it is a weighted-average with the temperature of the gas. Catalytic tests of fuel-rich combustion were run under pseudo-adiabatic conditions at fixed preheating (450 °C) and an overall pressure of P = 1.2 bar, using air as oxidant, unless otherwise stated. The thermal efficiency of the catalytic reactor was estimated to be 75% under typical conditions.

The effects of Rh loading, substrate material and morphology were studied at varying CH_4/O_2 ratio between 1.3 and 2.2, and keeping constant the total flow rate at 75 slph (standard liters per hour), corresponding to a gas hourly space velocity (GHSV) of 3.6×10^4 h^{-1} and to a residence time of about 25 ms at the average reactor temperature of 800 °C. Light-off temperatures were determined by ramping-up the external furnace under flow conditions at CH_4/O_2 = 1.8 and GHSV = 3.6×10^4 h^{-1}. The catalytic monoliths were tested after stabilisation upon exposure to standard reacting conditions.

Methane conversion and yields to CO and H_2 were calculated according to the subsequent definitions:

$$x_{CH_4} = 100\left(1 - \frac{{CH_4}^{OUT}}{CH_4^{OUT} + CO_2^{OUT} + CO^{OUT}}\right)$$

$$Y_{CO} = 100\left(\frac{CO^{OUT}}{CH_4^{OUT} + CO_2^{OUT} + CO^{OUT}}\right)$$

$$Y_{H_2} = \frac{100}{2}\left(\frac{{H_2}^{OUT}}{CH_4^{OUT} + CO_2^{OUT} + CO^{OUT}}\right)$$

based on the exit dry-gas mol fractions of CO, CO_2, CH_4 and H_2 independently measured by a continuous analyser with cross sensitivity correction (Hartmann & Braun Advance Optima). No other hydrocarbons except from methane were detected (by GC-FID/TCD analysis) in the products, whereas O_2 was always completely converted. Carbon and hydrogen balances were always closed within ±4%.

Thermodynamic equilibrium calculations were performed using CHEMKIN 4.1.1 software [14] generally among gaseous species only, having ruled out C formation on the catalysts.

2.3. Morphological and fluid dynamic considerations

Table 1 reports the main geometrical and corresponding fluid dynamic characteristics of the different supports tested.

Silicon carbide based substrates are characterized by enhanced thermal conductivity with respect to cordierite honeycombs (more than an order of magnitude) [15], higher maximum operating temperature (~1450 °C vs. 1250 °C) and linear expansion coefficient (5.0 vs. 1.7 mm/m at 1000 °C).

The void fraction (ε) depends on channel diameter (d_p) and wall thickness (t) of the substrates, and is around 60% for low cell density materials increasing up to about 85% for high cell density substrates with ultra thin walls (63 μm). The specific geometrical surface (S_v) depends on the inverse of d_p and is calculated according to the hollow cylinders model and depends linearly on ε.

Table 1
Geometric and fluid dynamic characteristics of the honeycomb supports tested.

Cell density (cpsi)	Material	Actual loading[a] (g/cm^3)	d_p (mm)	t (μm)	ε (%)	S_v (mm^{-1})	Re	L_{hy} (mm)	Pe_{ax}	Pe_{rad}	$k_g \times S_v \times 10^{-3}$ (s^{-1})
190	SiC (91%)	1.76	1.50	350	66	1.8	23	2.46	32	0.72	0.47
200	Cordierite	1.89	1.40	400	60	1.7	24	2.34	35	0.69	0.50
290	SiC (91%)	2.69	1.20	300	64	2.1	19	1.71	33	0.48	0.72
400	Cordierite	3.30	1.09	177	74	2.7	15	1.34	29	0.34	1.0
600	Cordierite	4.14	0.96	76	86	3.6	12	1.05	25	0.23	1.5
900	Cordierite	5.00	0.78	63	86	4.4	9	0.75	25	0.15	2.3
1200	Cordierite	4.85	0.67	63	83	5.0	9	0.64	26	0.11	3.0

d_p = channel diameter; t = wall thickness; S_v = specific geometrical surface; ε = open void fraction; k_g = O_2 mass transfer coefficient; L_{hy} = hydrodynamic entry length. $S_v = \frac{4\varepsilon}{d_p}$; $Pe_{ax} = \frac{\tau_{disp,ax}}{\tau_{conv}} = \left(\frac{L^2}{D}\right)\left(\frac{L}{u}\right)^{-1} = \frac{uL}{D}$; $Pe_{rad} = \frac{\tau_{disp,rad}}{\tau_{conv}} = \left(\frac{d_p^2}{D}\right)\left(\frac{L}{u}\right)^{-1} = \frac{ud_p^2}{DL}$; $\frac{L_{hy}}{d_p} = \frac{0.60}{0.035Re+1} + 0.056Re$; where L is monolith length, u the surface velocity, D the O_2 molecular diffusivity.
[a] Catalyst composition LMR-1.

Thus, S_v increases with cell density in the range 1.7–5 mm^{-1} (Table 1). Due to the fixed target average thickness of the washcoat layer, the actual loading of active phase deposited on the monoliths (Table 1) increases proportionally to their exposed surface area S_v. The effective Reynolds number (Re) calculated under the typical conditions of the experimental runs (with the linear velocity in the empty tube of 9 cm/s at standard conditions) is always below 25, corresponding to laminar flow. The hydrodynamic entry length L_{hy} for the development of a parabolic velocity profile increases with d_p, but, even in the case of low cell density monoliths, entrance effects do not extend beyond 25% of the total length of the honeycomb.

Remarkably, in the axial direction, the characteristic convection time is always sufficiently smaller than the dispersion time (axial Peclet number $Pe_{ax} > 25$), with the consequence that back-diffusion is negligible. On the other hand the radial Peclet (Pe_{rad}), defined as the ratio of the characteristic time of radial dispersion and of axial convection, varies in the range 0.11–0.72 increasing with channel dimension, thus suggesting that significant radial gradients should be expected particularly for monoliths with low cell density.

Table 1 also reports $k_g \cdot S_v$, where k_g is the average mass transfer coefficient calculated from the Hawthorn's correlation [16], which has a limited validity when a surface reaction takes place at the walls [17], but is a reasonable approximation for a rough estimation of mass and heat transfer efficiency. Resulting $k_g \cdot S_v$ values increase by a factor 6 passing from 200 to 1200 cpsi honeycombs.

3. Results and discussion

Elemental analysis by ICP was performed on powder and structured catalysts both as prepared and as used in catalytic oxidation tests: values of Rh content reported in Table 2 are very close to the nominal ones and no significant loss of noble metal was observed after exposure to high temperatures (peaks above 1000 °C) in the catalytic test.

XRD analysis did not show any signal of crystalline phases suggesting the presence of an amorphous oxide layer on the alumina support.

Values of BET specific surface area are reported in Table 2. The stabilized alumina used as catalyst support has a specific surface area of roughly 150 m^2/g after calcination in air at 800 °C and a mesoporosity of 0.25 cm^3/g with a mean pore diameter of 55 Å.

Addition of roughly 30 wt.% active phase (1%Rh-$LaMnO_3$) entails a reduction of the specific surface down to 80–90 m^2/g with a corresponding decrease in the total porosity and mean pore diameter down to respectively 0.16 cm^3/g and 40 Å. Ageing under partial oxidation reaction further reduces the surface area to 70 m^2/g.

DRIFT spectra of adsorbed CO did not evidence the presence of reduced Rh on the catalysts upon exposure to reaction up to 800 °C, in agreement with what observed for 1%Rh-$LaMO_3/Al_2O_3$ (M = Co or Mn) samples [11]. However, DRIFT analysis allowed the detection of hydrogen reducible Rh species. In fact bands of CO adsorbed detected on LMR-1 catalyst suggest that metal Rh species, giving rise to linear CO bonding (2056 cm^{-1}), appear already after reduction in H_2/N_2 at 450 °C, whereas new reduced Rh species providing the two typical gem-dicarbonyl bands at 2084 and 2016 cm^{-1} [18] are formed after reduction at 800 °C (Fig. 1).

TPR analysis was carried out for both powder and structured catalysts. Fig. 2 reports the comparison of H_2-TPR profiles of powder samples with 0.1, 0.5 and 1 wt.% rhodium content, respectively. All curves show a single main asymmetric reduction peak starting at roughly 140–150 °C and centred in the range 370–450 °C with a small shoulder at lower temperature, suggesting that reduction of both rhodium and manganese takes place in the same range.

At increasing the Rh content in the catalyst the main reduction peak becomes narrower and the temperature of the maximum (Table 2) progressively shifts towards lower values. The total H_2 consumption, also reported in Table 2, increases with Rh loading in the catalyst. If a complete reduction of rhodium from Rh^{3+} to metallic Rh is assumed, as suggested by DRIFT results, the

Table 2
ICP-MS, BET and H_2-TPR results for powder and selected structured catalysts.

Sample	Substrate	Rh by ICP[a] (w/w %)	BET[a] (m^2/g)	H_2 uptake[a] (mol H_2/g)	H_2/Mn[b] (mol/mol)	T_{max} (°C)
La-Al_2O_3		–	146	–	–	–
LMR-0.1		0.10	–	8.64×10^{-4}	0.68	452
LMR-0.5		0.50	–	9.59×10^{-4}	0.71	401
LMR-1		1.00	–	9.95×10^{-4}	0.68	369
LMR-1-290	SiC	1.01	90	1.14×10^{-3}	0.80	358
LMR-1-400	Cordierite	0.90	79 (70[c])	1.18×10^{-3}	0.83	354
LMR-0.5-600	Cordierite	0.48[c]	–	–	–	–
LMR-0.1-600	Cordierite	0.092[c]	–	–	–	–

[a] Referred to total weight of active phase, monolith substrate excluded.
[b] Assuming complete reduction of Rh^{3+} to Rh^0.
[c] After tests of self-sustained methane catalytic partial oxidation.

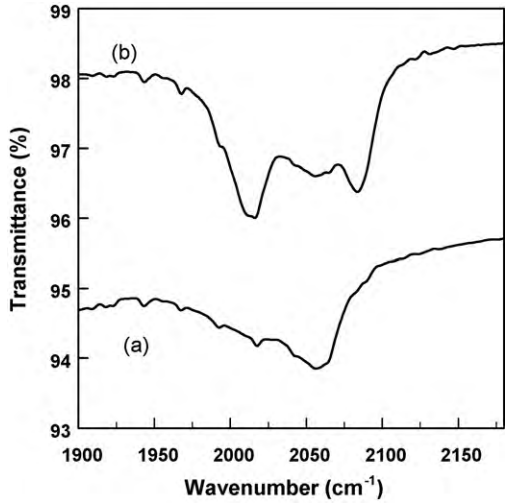

Fig. 1. DRIFT spectra of CO adsorbed on LMR-1 catalyst after reduction under H_2/N_2 flow at (a) 450 °C and (b) 800 °C.

corresponding H_2 consumption (stoichiometric H_2/Rh ratio = 1.5) can be subtracted from the total hydrogen uptake, in order to obtain the H_2/Mn ratio reported in Table 2. Very similar values are obtained for all the three samples corresponding to an initial average oxidation state of manganese between +3 and +4 and roughly 30% Mn^{4+}, which is typical of $LaMnO_3$, although its reduction does not occur in two steps as for the bulk perovskite [19]. In fact the narrow reduction peak detected for LMR catalyst is different from that observed for other supported $LaMnO_3$, extending in a wide range of temperature and clearly constituted by two or more partially overlapped signals [20], whereas is closer to that detected for manganese oxides. In particular, the maximum temperature is similar to that of the second reduction step of MnO_2 [20].

The presence of rhodium, although not affecting the extent of manganese reduction, strongly promotes its reducibility to Mn^{+2} even at low concentrations, most probably by a H_2-spillover mechanism. The strong interaction of Rh with Mn and the easier reduction of the transition metal oxide (which is proportional to Rh content) is likely the key to the better activity in methane partial oxidation of mixed Rh-$LaMnO_3$ formulation with respect to Rh or $LaMnO_3$ alone, especially in terms of light-off temperatures and syngas yields [11].

TPR profiles of monolith samples (1–400 cordierite and 1–290 SiC-based) with the same nominal composition but different substrate materials can be almost overlapped with the one of the corresponding powder catalyst (in Fig. 2 profile of 1–400 is reported for comparison). A slightly higher specific H_2 uptake was detected for both structured materials with respect to the powder sample that is most probably due to the additional reduction of some oxide species found in the formulation of the commercial honeycombs either as binders or impurities.

Nevertheless, it can be generally concluded that features of the powder catalysts are kept in the monolith samples and that the nature of the structured substrate does not affect the properties of the active phase. As a consequence, the differences observed in the catalytic performance between cordierite and SiC-based monoliths can be assigned to the variation in thermal conductivity of these two materials rather than to different properties of the active phase induced by the interaction with the substrate (see Section 3.2).

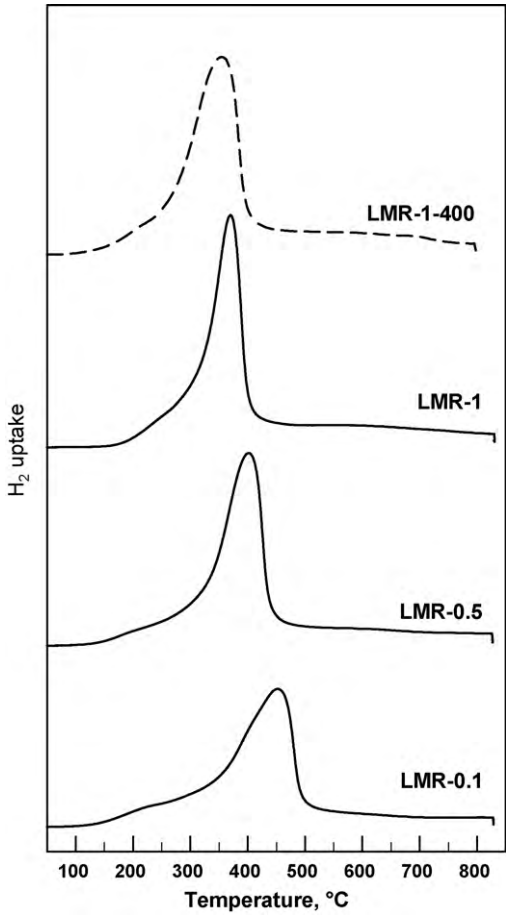

Fig. 2. H_2-TPR curves of LMR-*x* catalysts.

3.1. Pseudo-adiabatic catalytic tests

Low light-off temperature (i.e the minimum preheating temperature required for the catalyst to ignite the reacting mixture and self-sustain its catalytic oxidation at high conversion levels) is a key parameter in most combustion applications that invariably require easy ignition procedures with fast response and should avoid auxiliary devices such as pre-burners in order to get rid of their additional contribution to pollutants formation. In fact this is one of the main potential advantages of the fuel-rich catalytic combustion approach for ultra low NO_x gas turbine

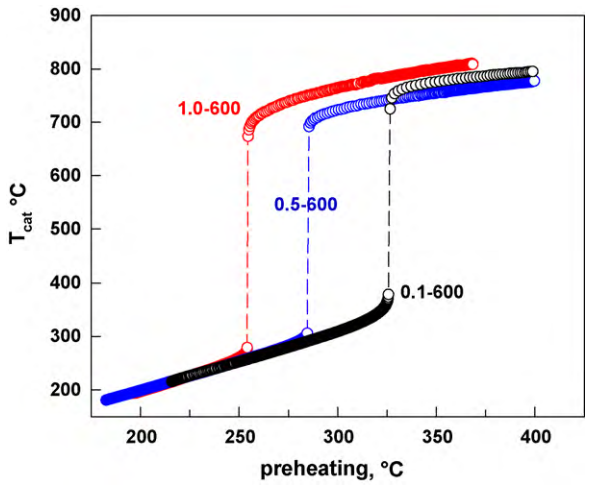

Fig. 3. Effect of Rh loading on light-off temperatures for self-sustained fuel-rich catalytic combustion over LMR-*x*-600 monoliths. CH_4/O_2 ratio = 1.8; GHSV = 36,000 h^{-1}.

technology with respect to the fuel-lean counterpart [1,3,10]. Fig. 3 shows the impact of Rh loading of LMR-*x*-600 catalysts on the ignition of methane-air mixtures of fixed feed ratio (CH_4/O_2 = 1.8): the light-off temperature increases with decreasing amount of noble metal, which represents the main active phase also at low temperature, passing from roughly 250 °C required for LMR-1 catalyst to 280 °C and 320 °C, respectively for LMR-0.5 and LMR-0.1. The reduction of light-off temperature on LMR catalysts follows the same trend of reducibility found by H_2-TPR and confirms a strong synergic interaction between phases. Indeed the promoting effect of the La–Mn mixed oxide phase enables to obtain roughly the same ignition performance of a 1%Rh/Al_2O_3 catalyst [11] on the LMR-0.5 sample with half the loading of noble metal. This is probably due to a faster depletion of molecular oxygen at low temperature by the Rh-$LaMnO_3$ catalyst, which can help to ignite and sustain the partial oxidation reactions also by *in-situ* heat generation.

Fig. 4 shows steady state catalytic performances of LMR-*x*-600 monoliths under pseudo-adiabatic conditions as a function of CH_4/O_2 feed ratio at fixed preheating (450 °C). For all the three systems methane conversion and yields to CO and H_2 follow the same qualitative trend of the corresponding adiabatic equilibrium curves calculated excluding C_s-formation, which, on the other hand, is thermodynamically predicted to occur for $CH_4/O_2 \geq 1.85$ (Fig. 4).

In particular, since O_2 is the limiting reactant, methane conversion progressively raises with decreasing CH_4/O_2 ratio (almost linearly down to 1.6–1.5), while both CO and H_2 yields pass through a maximum which occurs at CH_4/O_2 around 1.5. The catalytic performances (conversion and yields) of the three LMR-*x* catalysts follow the order of Rh loading and are very close for LMR-1 and LMR-0.5: characteristic experimental plots run almost parallel to each other and approach closer to the equilibrium values at lower feed ratios. Only CO yield slightly departs from the equilibrium even when methane conversion is almost complete, indicating some kinetic limitation that favours the formation of CO_2.

Comparing the results with those obtained on a reference 1%Rh/Al_2O_3 monolith [11] (Fig. 4), it can be seen that the synergy between Rh and La–Mn mixed oxide phase enables LMR-0.1 catalyst to give similar syngas yields even with a noble metal loading reduced to only 0.1%. Similar positive effects were reported with Rh-Ni bimetallic catalysts [9].

Table 3
Effect of Rh loading on the catalytic partial oxidation over LMR-*x*-600 monoliths at fixed feed ratio.

CH_4/O_2 = 1.8	LMR-1-600	LMR-0.1-600	Difference[a]
X_{CH_4} (%)	88.5	81.8	+6.7
Y_{H_2} (%)	79.3	68.5	+21.6 (10.8 × 2)
Y_{CO} (%)	78.1	70.5	+7.6
Y_{H_2O} (%)	9.2	13.3	−8.2 (−4.1 × 2)
Y_{CO_2} (%)	10.4	11.3	−0.9
T_{cat} (°C)	748	792	−44
T_{out} (°C)	618	634	−22

[a] Products molar flows per 100 CH_4 feed.

Regardless of Rh content, catalyst operated at a temperature level strictly controlled by oxygen availability in the range 700–1000 °C. It is worth noting that the reduction of the main active phase for partial oxidation (Rh) and the concurrent presence of a total oxidation catalyst such as the $LaMnO_3$ perovskite [20–22] does not appear to cause hot-spots or reactor overheating even at relatively high O_2 partial pressures.

Table 3 reports the difference in catalytic behaviour between LMR-1 and LMR-0.1 monoliths with extreme Rh contents at fixed feed ratio (1.8). It is observed that the increase of methane conversion is accompanied by a corresponding consumption of water of similar extent (in terms of molar flow rates at reactor exit normalized to a CH_4 feed of 100). At the same time more CO and H_2 are formed with a ratio close to 3. Those results strongly suggest that the over-performance of LMR-1 is related to its ability to catalyze much more efficiently the endothermic steam reforming reaction (1) between some unconverted methane and water produced in the first oxidation zone of the reactor [23,24].

$$CH_4 + H_2O \leftrightarrow CO + 3H_2 \quad \Delta H_r^0 = +206\,kJ\,mol^{-1} \tag{1}$$

This hypothesis is supported by the lower reaction temperature measured both in the catalyst and in the outlet gas even in correspondence of a higher methane conversion. Indeed Rh is reported to be a very active phase for steam reforming of methane

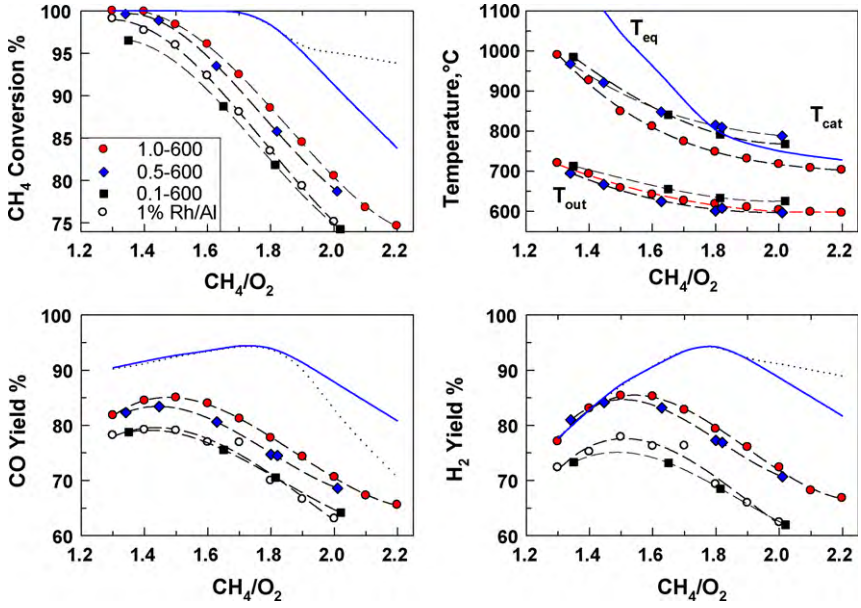

Fig. 4. CH_4 conversion, H_2 and CO yields and temperatures in the catalyst (T_{cat}) and in the exit gas (T_{out}) as a function of CH_4/O_2 feed ratio under self-sustained operation over LMR-*x*-600 monoliths with variable Rh loading. 1%Rh/Al_2O_3 on the same substrate from Ref. [11]. Solid lines correspond to equilibrium among gaseous species only, whereas dotted lines also include C_s-formation.

even at extremely short contact time (even below 1 ms) but not for dry reforming with CO_2 [23,24,27]. The slight reduction in CO_2 yield seems motivated by the occurrence of the slightly endothermic reverse water gas shift reaction (2), which also forms some additional CO by consuming an equivalent amount of H_2, rather than by any contribution from dry reforming [13,27].

$$CO_2 + H_2 \leftrightarrow CO + H_2O \quad \Delta H_r^0 = +41\ \mathrm{kJ\,mol^{-1}} \tag{2}$$

Such results are not limited to a single feed ratio even if the differences tend to disappear at lower values of CH_4/O_2 ratio, since methane conversion becomes complete also for the worst performing catalysts, and total oxidation products start to be favoured.

Indeed the temperature profiles reported in Fig. 4 suggest that best performing LMR-1 catalyst operates at slightly lower temperatures in the whole range of conditions explored. Heat losses in the post catalytic section of the reactor (cooling zone) and a measuring position too far away downstream of the catalyst prevent a more rigorous comparison among exit gas temperatures measured for the three catalysts and with the corresponding thermodynamic equilibrium temperatures. Nevertheless, LMR samples with higher Rh loading are better methane partial oxidation catalysts due to their ability to catalyze more steam reforming, which in turn appears to be kinetically controlled under the self-sustained reaction condition studied.

3.2. Effect of honeycomb substrate

The impact of substrate properties was studied for the best performing catalyst formulation (LMR-1). Fig. 5 compares catalysts on cordierite honeycombs with several cell densities with respect to CH_4 conversion and yields to CO and H_2.

A clear order of increasing performances can be established which follows the trend of cell densities from 200 to 1200 cpsi. The relevant experimental curves run almost parallel to each other and tend to merge in a single line reaching equilibrium values at the lowest feed ratios. Also the maximum in syngas yield moves towards higher values of CH_4/O_2 passing from 200 to 1200 cpsi and approaching closer to the equilibrium limit.

In fact, apart from the LMR-1-200 sample which displays a lower conversion, most significant differences among the samples are observed when comparing their CO and in particular H_2 yields. Similar effects were reported for Rh based foam catalysts [25] and spheres [26], with best syngas yields obtained for the smallest possible pore/diameter size.

As reported in Table 1, a larger cell density entails an increased exposed surface area S_v, which in turn guarantees an enhanced mass (and heat) transfer ($k_g \cdot S_v$), and also corresponds to a larger loading of active phase, which indeed more than doubles passing from 200 to 1200 cpsi. This is paid in terms of higher pressure drops for the same gas flow in smaller channels, which is a strong drawback especially for gas turbine combustors.

In the first oxidation zone of the Rh based catalytic honeycombs the reaction is mass transfer limited [24]; as a consequence this oxidation zone is progressively shortened by increasing the cell density, thus leaving a larger fraction of the catalytic reactor to the steam reforming zone. Steam reforming of residual methane from the oxidation zone is mainly controlled by the surface kinetics, thus it is favoured on high cell density honeycombs by the higher amount of deposited active phase and longer contact times.

The enhancement of the gas–solid heat transfer also plays an important role in favouring high cell density honeycombs since severe heat transport limitations occur along the catalyst axis [24]. In the oxidation zone, heat generation occurs at the catalyst surface whose temperature is much higher than the cold incoming gases

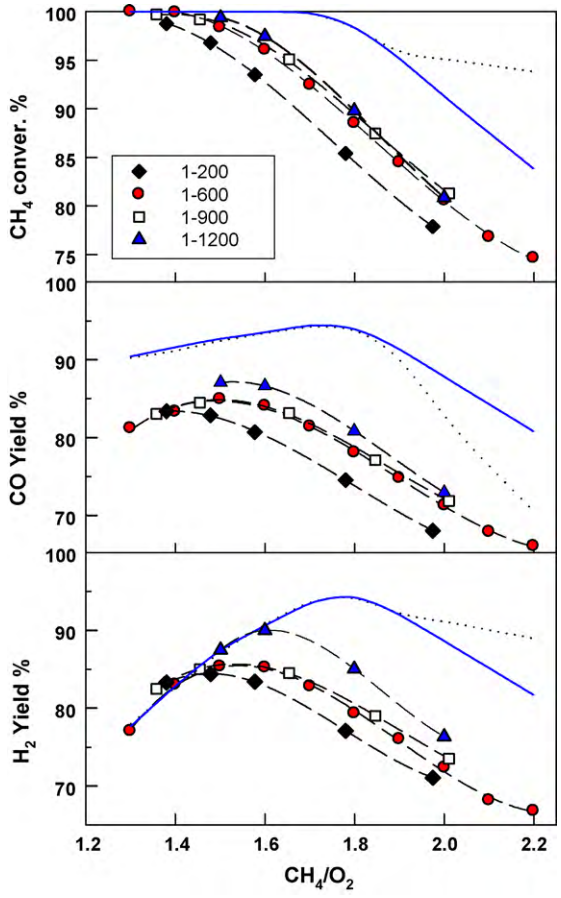

Fig. 5. CH_4 conversion, CO and H_2 yields as a function of CH_4/O_2 feed ratio over LMR-1-*y* cordierite honeycombs with different cell density. Solid lines correspond to equilibrium among gaseous species only, whereas dotted lines also include C_s-formation.

which are progressively heated by convection moving along the monolith. Due to the higher heat transfer efficiency for a catalytic monolith with smaller d_p the wall temperature rises more slowly and its peak point is shifted downstream [21].

The situation is reversed in the steam reforming zone, where the endothermic surface reaction cools the catalyst faster than heat is transferred from the now hot gases to the solid structure. In this case a higher gas–solid heat transfer efficiency enables to self-sustain the endothermic reaction in the second part of the reactor through a better heat management. Moreover the magnitude of hot-spots (defined as the maximum difference between surface and gas temperatures) is reduced [21] which is beneficial for catalyst durability.

It is evident that such description of the phenomena neglects the heat transport along the flow direction by conduction (and radiation) inside the solid matrix of the honeycombs, which is a reasonable approximation for low thermal conductivity substrates such as cordierite [17,27], in particular when dealing with ultra thin walls monoliths.

Nevertheless, a more effective heat management of the catalytic reactor can be obtained with a different substrate material characterized by enhanced solid thermal conductivity. Fig. 6 compares the performance of cordierite (LMR-1-200) and SiC-based (LMR-1-190) honeycombs with similar geometric and fluid dynamics properties and active phase loading (Table 1), which only differ for the higher (10×) solid thermal conductivity of the latter. Methane conversion, CO and H_2 yields are enhanced on the SiC-based honeycomb in the whole range of feed ratio

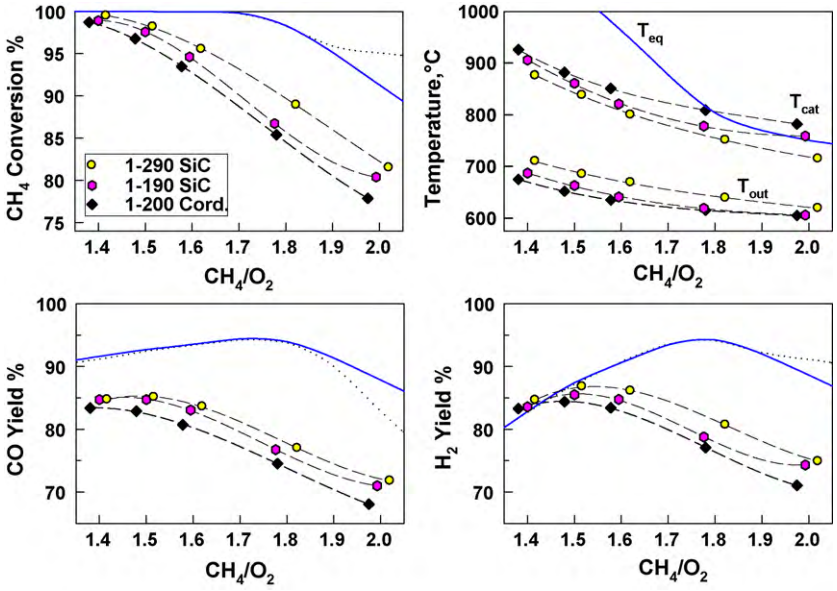

Fig. 6. CH_4 conversion, H_2 and CO yields and temperatures in the catalyst (T_{cat}) and in the exit gas (T_{out}) as a function of CH_4/O_2 feed ratio under self-sustained operation over LMR-1-*y* honeycombs of different materials (SiC and cordierite). Solid lines correspond to equilibrium among gaseous species only, whereas dotted lines also include C_s-formation.

explored. Moreover the temperatures measured in the middle of the catalyst are always higher for the cordierite honeycomb, whereas gas temperatures are higher at the exit of the SiC-based monolith, thus suggesting the reduction of catalyst peak temperature and a flat axial profile related to a more efficient heat transport from the oxidation towards the reforming zone of the reactor. Performance data of LMR-1-290 sample (Fig. 6) confirm that the increase in the cell density of honeycombs is effective to enhance syngas yield also in the case of SiC-based material.

To gain further insight into the effect of the higher solid thermal conductivity of the substrate an experiment with oxygen as oxidant (instead of air) was performed at $CH_4/O_2 = 1.7$, using a moveable thermocouple for spatial temperature measurements along the axial coordinate of the catalyst. As evident from Fig. 7 the cordierite honeycomb with low thermal conductivity displays a sharp maximum of roughly 1200 °C (very close to the maximum sustainable value for the material) attained within the first 2 mm from the reactor inlet section. Thereafter the temperature quickly decreases with the second half of the reactor operating between 930 and 850 °C. On the other hand the SiC-based honeycomb catalyst shows a rather flat temperature profile, with a smaller maximum of 1057 °C attained at 4 mm from the entrance. Overall this catalyst operates with a second reactor zone 80 °C hotter than the corresponding sample with cordierite monolith, as also confirmed by the higher temperature of exit gases.

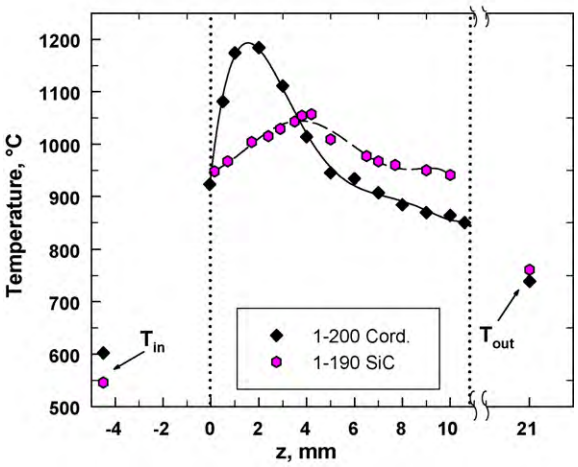

Fig. 7. Temperature profiles along the axial coordinate of LMR-1-190 (SiC) and LMR-1-200 (cordierite) honeycomb catalysts during self-sustained partial oxidation reaction at CH_4/O_2 feed ratio = 1.7, using O_2 as oxidant; GHSV = 36,000 h^{-1}.

Table 4 compares the catalytic partial oxidation performances corresponding to the temperature profiles of Fig. 7. It is seen that methane conversion is higher on SiC-based honeycomb, as well as H_2 and CO yields. Once again the surplus hydrogen appears to be formed mainly by reaction of methane with water through the steam reforming, since the ratio of the variation in flows for H_2 to CH_4 is close to 3 and for H_2 to CO well above 2. It seems confirmed that the higher temperatures achieved in the second part of the LMR-1-190 catalyst due to increased heat flow from the oxidation zone speed up steam reforming, while also favouring the reverse water gas shift reaction consuming some CO_2 and H_2. It is also evident that higher catalyst temperature in the first oxidation zone of the reactor can shift the selectivity more towards partial oxidation products reflecting the thermodynamic trend [24]; through this way the "feed" to the following steam reforming reactor zone is also changed.

Table 4
Effect of honeycomb substrate material on catalytic partial oxidation reaction at CH_4/O_2 feed ratio = 1.7, using O_2 as oxidant; GHSV = 36,000 h^{-1}.

$CH_4/O_2 = 1.7$	LMR-1-190 (SiC)	LMR-1-200 (cordierite)	Difference[a]
X_{CH_4} (%)	98.5	95.8	2.7
Y_{H_2} (%)	94.1	90.4	7.4 (3.7 × 2)
Y_{CO} (%)	92.6	89.2	3.4
Y_{H_2O} (%)	4.4	5.4	−2.0 (−1.0 × 2)
Y_{CO_2} (%)	5.9	6.6	−0.7
T_{max} (°C)	1057	1184	−127
T_{10mm} (°C)	942	864	78
T_{out} (°C)	761	739	22

[a] Products molar flows per 100 CH_4 feed.

4. Conclusions

Experimental results showed that mixed Rh-$LaMnO_3$ catalysts are suitable for fuel-rich combustion applications, showing positive synergetic effects linked to enhanced redox behaviour that ensure relatively high methane conversion and syngas yields even at reduced Rh loadings. However, a progressive reduction of light-off temperature and a parallel improvement of the catalytic partial oxidation performance under pseudo-adiabatic operation are observed by increasing Rh content in the LMR catalysts, which appears mainly due to the larger contribution from steam reforming reaction in the second part of the honeycombs. For the same reason it is possible to obtain further improvements by optimization of process conditions through the proper choice of the honeycomb morphology and material. High cell density substrates characterized by a larger exposed surface area and a higher active phase loading promote the occurrence of steam reforming reaction which is largely kinetically controlled. Moreover their higher gas–solid heat transfer efficiency favours a better reactor heat management, reducing solid hot-spots and sustaining a higher temperature level in the steam reaction zone with the heat generated in the oxidation zone. However, the choice of optimal support should be driven by a tradeoff analysis among catalytic performance, pressure drops, structural strength and ease of catalyst deposition.

A similar improvement of heat management was possible in the case of high solid thermal conductivity substrates, whose better catalytic performances are obtained owing to a relatively flatter reactor temperature profile, with higher temperatures towards the exit which speed up reaction in the reforming zone.

References

[1] D. Ciuparu, M. Lyubovsky, E. Altman, L. Pfefferle, A. Datye, Catal. Rev. 44 (2002) 593.
[2] T. Furuya, K. Sasaki, Y. Hanakata, T. Ohhashi, M. Yamada, T. Tsuchiya, Y. Furuse, Catal. Today 26 (1995) 345.
[3] M. Lyubovsky, L. Smith, M. Castaldi, H. Karim, B. Nentwick, S. Etemad, R. LaPierre, W. Pfefferle, Catal. Today 83 (2003) 71.
[4] B.C. Enger, R. Lødeng, A. Holmen, App. Catal. A: Gen. 346 (2008) 1.
[5] P.D.F. Vernon, M.L.H. Green, A.K. Cheetham, A.T. Ashcroft, Catal. Lett. 6 (2) (1990) 181.
[6] K.L. Hohn, L.D. Schmidt, Appl. Catal. A: Gen. 211 (2001) 53.
[7] L.V. Mattos, E.R. de Oliveira, P.D. Resende, F.B. Noronha, F.B. Passos, Catal. Today 77 (2002) 245.
[8] L. Majocchi, G. Groppi, C. Cristiani, P. Forzatti, L. Basini, A. Guarinoni, Catal. Lett. 65 (2000) 49–56.
[9] F. Basile, G. Fornasari, F. Trifirò, A. Vaccari, Catal. Today 77 (2002) 215.
[10] M. Lyubovsky, S. Roychoudhury, R. Le Pierre, Catal. Lett. 99 (2005) 113.
[11] S. Cimino, G. Landi, L. Lisi, G. Russo, Catal. Today 117 (2006) 454.
[12] D. Jollie, Platinum 2008, www.platinum.mattey.com.
[13] S. Cimino, G. Landi, L. Lisi, G. Russo, Catal. Today 105 (2005) 718.
[14] R.J. Kee, F.M. Rupley, J.A. Miller, M.E. Coltrin, J.F. Grcar, E. Meeks, H.K. Moffat, A.E. Lutz, G. Dixon-Lewis, M.D. Smooke, J. Warnatz, G.H. Evans, R.S. Larson, R.E. Mitchell, L.R. Petzold, W.C. Reynolds, M. Caracotsios, W.E. Stewart, P. Glarborg, C. Wang, O. Adigun, Chemkin Collection, Release 4.0, Reaction Design, Inc., San Diego, CA, 2004
[15] J.P. Joulin, B. Cartoixa, J.B. Dementhon, T. Becue, B. Martin, SAE paper 01-2029 (2004).
[16] R.D. Hawthorn, AIChE Symp. Ser. 70 (1974) 428.
[17] G. Groppi, E. Tronconi, P. Forzatti, Catal. Rev. Sci. Eng. 41 (1999) 227.
[18] S. Trautmann, M. Baerns, J. Catal. 150 (1994) 335.
[19] L. Lisi, G. Bagnasco, P. Ciambelli, S. De Rossi, P. Porta, G. Russo, M. Turco, J. Solid State Chem. 146 (1999) 176.
[20] S. Cimino, S. Colonna, S. De Rossi, M. Faticanti, L. Lisi, I. Pettiti, P. Porta, J. Catal. 205 (2002) 309.
[21] F. Donsì, S. Cimino, A. Di Benedetto, R. Pirone, G. Russo, Catal. Today 105 (2005) 551.
[22] A.B. Mhadeshwar, D.G. Vlachos, Ind. Eng. Chem. Res. 46 (2007) 5310.
[23] T. Liu, C. Snyder, G. Veser, Ind. Eng. Chem. Res. 46 (2007) 9045.
[24] R. Horn, K.A. Williams, N.J. Degenstein, A. Bitsch-Larsen, D. Dalle Nogare, S.A. Tupy, L.D. Schmidt, J. Catal. 249 (2007) 380.
[25] A.S. Bodke, S.S. Bharadwaj, L.D. Schmidt, J. Catal. 179 (1998) 138.
[26] S. Specchia, G. Negro, G. Saracco, V. Specchia, App. Catal. B: Env. 70 (2007) 5.
[27] A. Schneider, J. Mantzaras, P. Jansohn, Chem. Eng. Sci. 61 (2006) 4634.